

Drifter measurements in a laboratory rip current

Andrew B. Kennedy and David Thomas

Department of Civil and Coastal Engineering, University of Florida, Gainesville, Florida, USA

Received 23 April 2003; revised 21 April 2004; accepted 18 May 2004; published 7 August 2004.

[1] This paper investigates circulation in a laboratory rip current system using large numbers of Lagrangian drifters, with supplementary current meter and water level measurements. These represent the most dense measurements to date of laboratory rip circulation over a large spatial area. Overall, circulation is found to be very unsteady, with strong changes in circulation apparent at many length and time scales. Drifter and current meter measurements are compared in the rip channel, and Stokes drift is found to be a significant component of drifter velocities in this region. Estimated generation of circulation is compared with computed bottom friction dissipation, with good agreement. The mean cellular circulation about a dividing streamline is found to be surprisingly small when compared with computed rates of generation of circulation. Finally, the divergence of volume flux computed using drifters is found to be significant, with depth-varying wave-induced mass transport, depth-varying Eulerian velocities, and velocity/drifter concentration effects the likely sources of error. *INDEX TERMS:* 4546 Oceanography: Physical: Nearshore processes; 4512 Oceanography: Physical: Currents; 4560 Oceanography: Physical: Surface waves and tides (1255); 4594 Oceanography: Physical: Instruments and techniques; *KEYWORDS:* rip currents, nearshore processes, circulation

Citation: Kennedy, A. B., and D. Thomas (2004), Drifter measurements in a laboratory rip current, *J. Geophys. Res.*, 109, C08005, doi:10.1029/2003JC001927.

1. Introduction

[2] In recent years there has been significant interest in topographically controlled rip current systems. Part of this stems from intrinsically interesting features in their behavior, while the danger rip currents pose also gives them practical importance.

[3] Early observations were made by *Shepard et al.* [1941], who described narrow, agitated, sediment-laden currents flowing seaward from the beach. These were related to both natural and manmade inhomogeneities in topography. Shepard also introduced a basic description of rip currents that persists to this day, with shore-parallel feeder currents, strong offshore flow in the rip neck, an expanding head, and gentle return flow. Additional observations indicated that the rip became a surface current as it flowed offshore. Scattered investigations in subsequent years [*Shepard and Inman*, 1950; *McKenzie*, 1958; *Sonu*, 1973; *Brander and Short*, 2001] added more description and have presented mainly empirical correlations between environmental conditions and rip current properties. Field observations have had relatively sparse fixed instrument or drifter density because of the cost and difficulty of dense coverage. In general, rip currents were observed to be strongest for larger wave heights and/or low tidal levels.

[4] With the discovery of wave-induced radiation stress [e.g., *Longuet-Higgins and Stewart*, 1964], it became pos-

sible to understand rip currents in more detail, allowing direct computations. Early work by *Bowen* [1969], *Noda* [1972], and *Ebersole and Dalrymple* [1980], among others, showed that gradients in radiation stresses on uneven topography created circulation cells which resembled rip currents. More sophisticated recent modeling efforts include *Sørensen et al.* [1998], *Chen et al.* [1999], *Haas and Svendsen* [2000], and *Yu and Slinn* [2003]. Although computational details differ significantly, all recent computations show quite complex behavior; highly unsteady currents shedding eddies offshore, strong vorticity in the area of the rip channel, and strong wave-current interaction. This unsteady behavior was first noted in laboratory experiments by *Haller and Dalrymple* [2001], who identified it as a jet instability and found reasonable agreement between predicted and measured periods of oscillation. This unsteady motion exists even when wave forcing is purely monochromatic.

[5] Laboratory studies of topographically forced rip currents began at a somewhat later date than other approaches. Studies by *Hamm* [1992], *Drønen et al.* [1999, 2002], *Haller and Dalrymple* [2001], *Kennedy and Dalrymple* [2001], *Haas and Svendsen* [2002], and *Haller et al.* [2002] have provided valuable information on forcing, circulation, and instabilities. However, because most instruments are fixed, with limited numbers, it has proved difficult to obtain dense data over large areas. Furthermore, comparison and confirmation of numerical predictions such as vortex generation and shedding is very difficult using fixed instruments. *Drønen et al.* [2002] used sinking drifters in a half-rip current setup, but convergences in bottom

velocity tended to strand the drifters near the location of breaking in the rip channel.

[6] Here, we attempt to remedy some of these limitations by measuring laboratory rip current circulation using Lagrangian drifters with weak positive flotation. Supplementary measurements use acoustic doppler velocimeters (ADV) and capacitance-type surface measurements. Experiments were performed on the rip current topography of *Haller and Dalrymple* [2002], which has seen more study than any other laboratory setup. Advantages of Lagrangian measurements include greater coverage and easy computation of material derivatives. Disadvantages include the difficulty of obtaining time-varying properties at a given location. Here we concentrate on general properties and mean circulation of the rip current; future publications are to examine other aspects.

[7] In the first comprehensive studies of rip currents, *Shepard et al.* [1941] and *Shepard and Inman* [1950] used in part floating drifters to map out the basic circulation patterns and velocities, a task which would have been very difficult using fixed current meters. This approach has been used in whole or in part by several other field investigators throughout the years, with $O(10)$ drifters proving suitable for a basic representation of the circulation cell [*Sonu*, 1973; *Huntley et al.*, 1988; *Brander and Short*, 2001]. To provide a denser or time-varying estimate of the circulation might require an increase to $O(100)$ s of drifters. In field measurements this would be a significant difficulty, but for laboratory investigations it is not a major obstacle.

[8] In some ways, laboratory drifter measurements in waves are considerably different from the more common Eulerian measurements by fixed instruments. It is well known that a fluid particle position averaged over one wave period has a net transport in the direction of wave travel that is in addition to any current measured by a fixed current meter [e.g., *Dean and Dalrymple*, 1984]. This means that a measured particle velocity is

$$\mathbf{U}_D = \mathbf{U}_E + \mathbf{U}_{SL}, \quad (1)$$

where \mathbf{U}_E is the two-dimensional (2-D) Eulerian velocity at the mean particle position averaged over a wave period and \mathbf{U}_{SL} is the wave Lagrangian drift, which may be composed of both an irrotational Stokes velocity and additional roller transport under breaking waves. Current meters can only measure Eulerian components of the velocity. Thus care must be taken in interpreting results, as velocities using drifters can be somewhat different from results using Eulerian current meters.

[9] If both Eulerian velocity and wave Lagrangian drift are constant over depth, then the drifter velocity is equal to the overall mass transport velocity, defined as

$$\begin{aligned} \mathbf{U} &\equiv \frac{\mathbf{M}}{h + \eta} \\ \mathbf{M} &\equiv \int_{-h}^{\eta} \mathbf{u} dz, \end{aligned} \quad (2)$$

where h is the still water depth, η is the instantaneous surface elevation, \mathbf{u} is the instantaneous horizontal water

velocity vector, and the overline denotes averaging over a wave period. Small-amplitude wave theory suggests that nonbreaking waves in shallow water have Lagrangian drift that is independent of depth [e.g., *Dean and Dalrymple*, 1984], so floating drifter velocities may be a good approximation to mass transport velocities in shallow water. Since mass transport velocities are widely used in theories of nearshore hydrodynamics [e.g., *Mei*, 1983], this is of considerable importance, and we will approximate mass transport velocities here by surface drifter velocities which have been low pass filtered to remove wave orbital velocities. In deeper water, at locations with depth varying currents, and where finite amplitude effects (e.g., breaking) cause departures from small amplitude wave theory, this representation will show increasing error.

2. Experimental Setup

[10] Tests were conducted in the multidirectional wave basin at the Center for Applied Coastal Research at the University of Delaware; this is the same location for rip current studies by *Haller and Dalrymple* [2001], *Kennedy and Dalrymple* [2001], and *Haas and Svendsen* [2002]. These references may be consulted for a complete description of the basin and rip current topography. Figure 1 shows a schematic of the basin, indicating the field of view for the video camera. Three acoustic doppler velocimeter (ADV) current meters were located at $x = 11.8$ m at the centerline of the measured rip channel and 20 cm on either side, and a wave gauge was at $x = 6$ m, $y = 16.2$ m; however these were never in place simultaneously with drifter tests, as they would have interfered with the drifters and obscured tracking.

[11] Figure 2 shows a photograph of one of the drifters used, which were actually swimming pool lane dividers with diameter $d = 10.7$ cm, thickness $w = 1.7$ cm, and small positive flotation. Where waves were small, drifters were believed to track flow well. In the surf zone, drifters did not “surfboard” to the shoreline as would objects with strong flotation. However, they were influenced by breaking waves to a degree which, although unmeasured, appeared significant.

[12] The series of tests presented here examined steady state conditions over longer times. The concept of steady state conditions can only be applied to rip currents stochastically, as they are unsteady even in the absence of unsteady forcing, but long measurements can give good estimates of mean and time-varying properties. Table 1 lists test conditions. Test identifiers are composed of four groups: “S” or “Gxx,” denoting steady waves or a group length of “xx” waves, respectively; “H” or “L,” denoting high or low water conditions; a number giving the wave period in seconds; and finally “M” or “L,” a qualitative indication of medium or large wave heights.

[13] Drifters were tracked at 3 Hz using captured images from a shore-mounted video camera. Image coordinates were then rectified to still water level Cartesian coordinates. Figure 3 shows an example of a captured image, with drifters. It proved necessary to take into account refraction through the water column when quantifying the apparent location of the ground control points with known location (these are seen as cross marks in Figure 3). Several rectification schemes were tested; differences were in general of $O(1)$ pixel). The final scheme, for which all quantitative

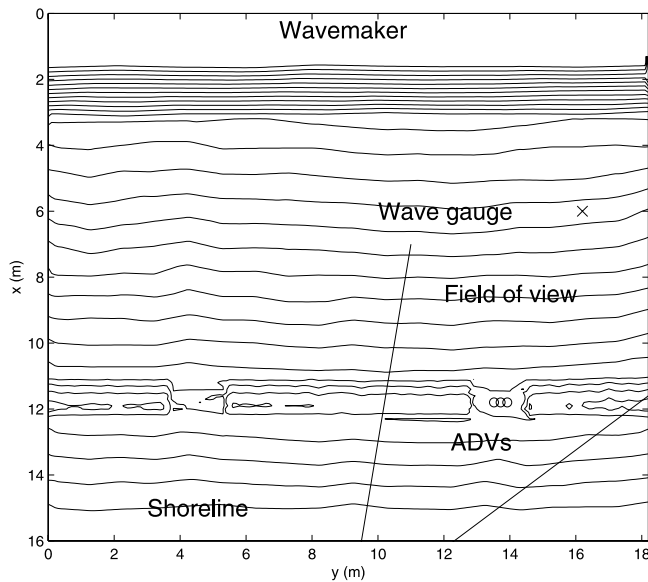


Figure 1. Schematic of setup for laboratory experiments, showing 2.5 cm evenly spaced depth contours.

results are presented here, used a slightly modified direct linear transformation (DLT) [see, e.g., *Holland et al.*, 1997]. Because the DLT scheme as implemented required only six points to determine all properties and 59 ground control points were available, the system was massively overdetermined and was solved in a least squares sense.

[14] For systems with very many visible small particles, techniques such as particle image velocimetry (PIV) work well. Here, drifters were much larger and more widely spaced than is optimal for PIV, so they were tracked directly. Direct tracking has certain advantages; Lagrangian paths give conclusive proof of flow patterns, and all velocity errors must be high frequency when a discrete object is tracked for a long time.

[15] A semiautomatic tracking procedure was devised, where the mean image was subtracted from every individual image, making the drifter more visible as a dark object in a light and generally featureless background. A cutoff filter was then applied, where pixels darker than a given threshold were left unchanged, but pixels lighter than this were set to

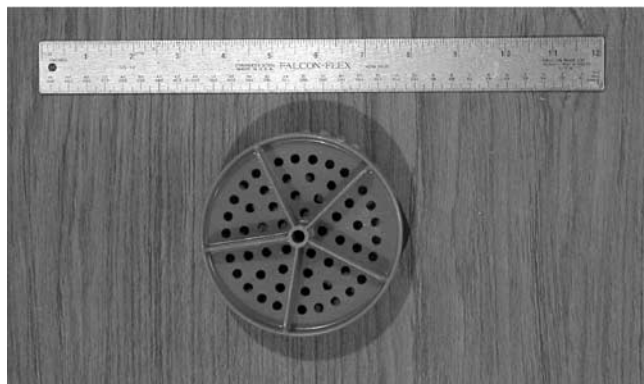


Figure 2. Lagrangian drifter used in experiments. See color version of this figure in the HTML.

Table 1. Test Conditions, Where M Indicates Monochromatic Waves

Test	RMS Wave Height, cm	Group Period, s	Wave Period, s	Bar Depth, cm	Particles Tracked
G32H1M	4.32	32	1	4.73	239
SH1M	4.28	M	1	4.73	293
G32L1M	4.62	32	1	2.67	204
SL1M	4.83	M	1	2.67	241
SH1L	6.18	M	1	4.73	356
SL133L	5.22	M	1.33	2.67	158
G64H1M	3.69	64	1	4.73	310
SH267M	3.97	M	2.67	4.73	221

a uniform bright value, which was taken as the zero datum for center of mass considerations. This further emphasized the dark drifters over the lighter background.

[16] The drifter was then followed automatically by computing the center of mass coordinates of the dark drifter over an interrogation window of specified size. The central coordinates of this window were chosen by linearly extrapolating the previous two coordinates. When drifters came too close to each other or sometimes when they changed directions suddenly or traveled into lighting reflections, tracking was manually assisted. All drifters were tracked in the image domain, and image coordinates were subsequently rectified to the Cartesian still water level. Drifter tracks were then zero-phase, low-pass filtered at a rate of 0.33 Hz. This removed effects of both wave orbital velocities and tracking errors and appeared to have a negligible effect on low-frequency flow. To test the effect of errors in manual tracking assistance, one test was tracked twice using the same input videotape. Mean velocities were compared and found to be almost identical, confirming that the manual interventions had a negligible effect on the end result.

[17] Steady state tests covered a range of conditions, as shown in Table 1. Wave height, water level, wave period, and wave unsteadiness were all varied to test their effect on circulation. Unsteady waves were actually bichromatic around the given central frequency. All bichromatic tests here used $a_1 = 2a_2$, where a_1 and a_2 are the amplitudes of the two components.

[18] The test series may in some ways be thought of as a perturbation about test SH1M, with monochromatic 1 s

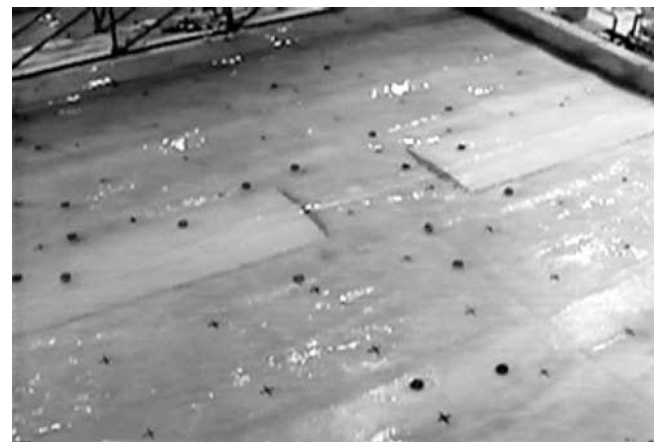


Figure 3. Sample of captured video image, with drifters. See color version of this figure in the HTML.

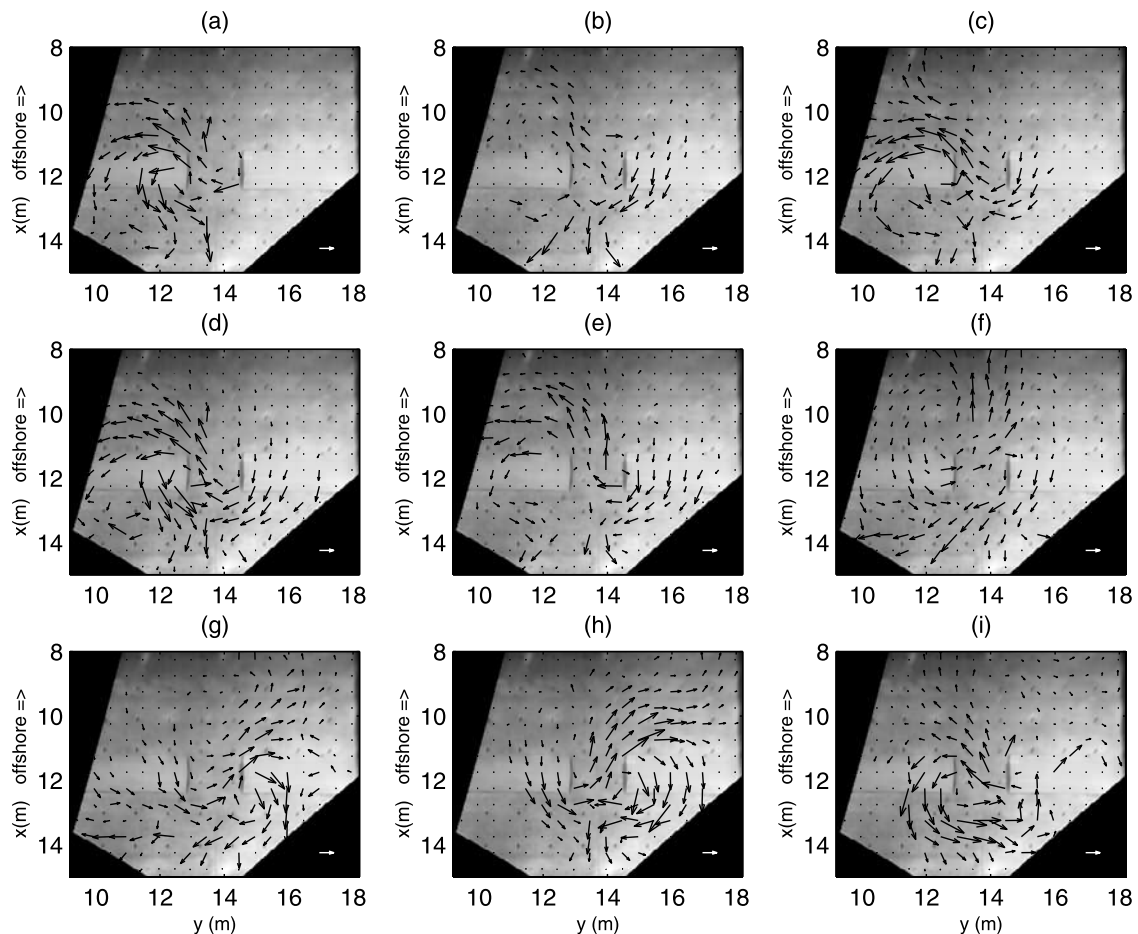


Figure 4. Two minute averages of drifter velocities over the first 18 min of test G32H1M. Shoreline is at bottom of picture and the arrows at bottom right have magnitude 10 cm/s.

waves and a deeper water level. Compared with this, tests G32H1M and G64H1M have unsteady forcing with similar other characteristics, test SL1M has a lower water level, test G32L1M has both lower water and unsteady forcing, test SH1L has larger waves, test SH267M has a different wave period, and test SL133L has a different water level, height, and wave period.

[19] Perhaps the greatest uncertainty in these tests resulted from the time period analyzed. Software limitations imposed an 18.2 min maximum observation length (32,768 samples at 30 Hz), which in many cases appeared to be sufficient for averaging the unsteadiness seen in all tests on many different temporal and spatial scales, in the presence and absence of unsteady wave forcing. However, some high water tests appeared to have very low-frequency motion of $O(10-25)$ min where the rip current would change its direction left or right. As described in section 4, this introduced some error in the computation of mean velocities. This is despite the fact that these correspond to a nearly 2 hour measurement period in the field, using appropriate Froude scaling.

3. General Behavior

[20] Even before examining mean properties, it is useful to consider the general behavior of the system, which

showed many scales of motion. Circulation cell scales of $O(2.5-10)$ m were always visible, where the water traveling offshore in the rip channel would return over the bar to shallow water. Larger-scale circulation, which produced significant mixing between the left and right rip currents, could be seen in many cases. Sometimes the rip would suddenly change direction from left to right for no apparent reason. Figure 4 shows an example from test G32H1M where a strong leftward trend suddenly changed to a rightward trend. Velocities (computed using a binning approach to be described later) are given only at locations where drifters pass by during each 2 min period. These shifts could have very long periods of oscillation; here it appears to be of $O(15-25)$ min and did not look much like an oscillating jet. Such sudden changes in velocity have been previously observed by current meters on this topography. For waves with slightly different conditions than tests G32H1M and SH1M, *Haller and Dalrymple* [2001] found low-frequency oscillations of $O(200)$ s, which is a somewhat higher frequency than found here. The present results are not necessarily incompatible with Haller and Dalrymple's observations; very low-frequency oscillations are more obvious on path lines, and Haller and Dalrymple did find significant energy at frequencies lower than the peak. Also, *Haas et al.* [2003] performed computations over this topography for conditions fairly similar to test

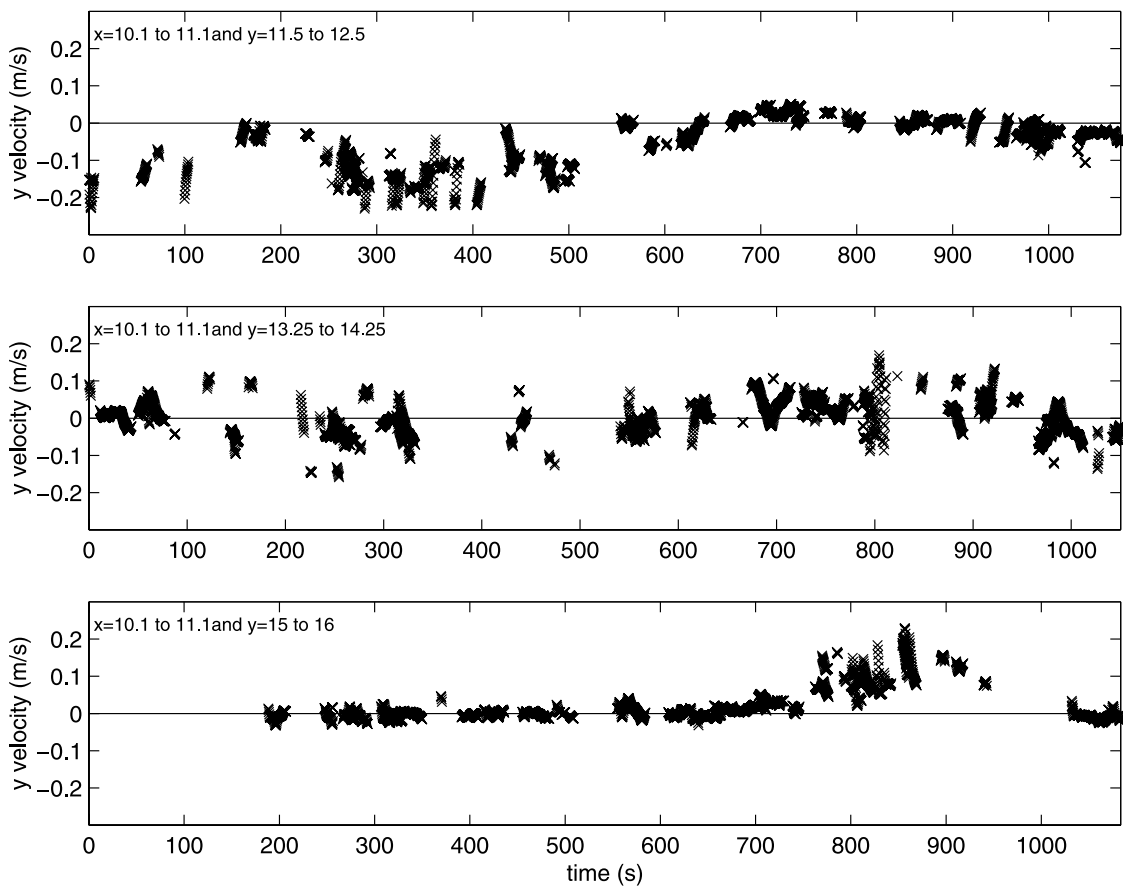


Figure 5. Test G321M drifter velocities just offshore of the bar in bins (a) left of rip channel, (b) offshore of rip channel, and (c) right of rip channel.

G32H1M, found low-frequency fluctuations of $O(4-500)$ s, and related these to wave-current interaction and its influence on wave breaking patterns.

[21] Because drifters traveled in and out of any area of interest at irregular intervals, it proved impossible to obtain continuous time series of velocity, even in the most densely populated regions. However, even incomplete time series show interesting phenomena. Figure 5 shows time series of drifter velocities for test G32H1M, longshore velocities for all drifters instantaneously in $1\text{ m} \times 1\text{ m}$ bins just offshore of the bar. For times less than around 10 min, the bin to the left of the rip channel (for an observer on the beach and facing offshore) shows strongly negative longshore velocities, while the rightward bin shows almost zero velocity. A sudden change gives strong positive velocities to the right of the rip channel, while velocities on the left side drop to near zero. Comparisons of Figures 4 and 5 show that the changes in measured drifter velocities are due to changes in cell-scale circulation; as the direction of the rip current changes so do the drifter velocities. Thus cellular-scale instabilities appear to be the cause of at least some low-frequency velocity oscillations.

[22] Not all tests resembled test G32H1M in its low-frequency behavior. Figure 6 shows 2 min mean velocities from test G32L1M, which was like test G32H1M except for a lower water level. Although low-frequency motion is visible, it is not as strong as seen in test G32H1M. The

rip here looks more or less symmetric over the 2 min scales of most pictures; most unsteadiness appears to be on a shorter time scale.

[23] The analysis of *Haller and Dalrymple* [2001] test C (which is broadly comparable to test G32L1M here, with small differences in wave height and steady instead of unsteady forcing) found a peak jet oscillation period of around 55 s. Again, an oscillation this short is not resolvable on our 2 min means, but Haller and Dalrymple did note significant energy below the peak jet oscillation frequency in many tests.

[24] Figure 7 presents unsteady properties for test SH267M using drifter paths instead of 2 min velocities, which allows finer scales to be resolved. As in test G32H1M, very long term oscillations are visible. This is not surprising, as water levels and mean velocities are similar, but is not our focus. Instead, we emphasize three phenomena: areas of strong recirculation between the bars and the shoreline, numerous traces of vortices of $O(0.5\text{ m})$ being shed offshore (e.g., top left of Figure 7e), and evidence of large vortices of $O(1.5\text{ m})$ leaving their positions around the bar and rip channel, and moving offshore (Figures 7b and 7i). Large vortex shedding was more apparent in this test than any other and appears to be associated with changes in direction of the rip current. Vortex shedding in rip current topographies has been predicted numerically in several studies [*Chen et al.*,

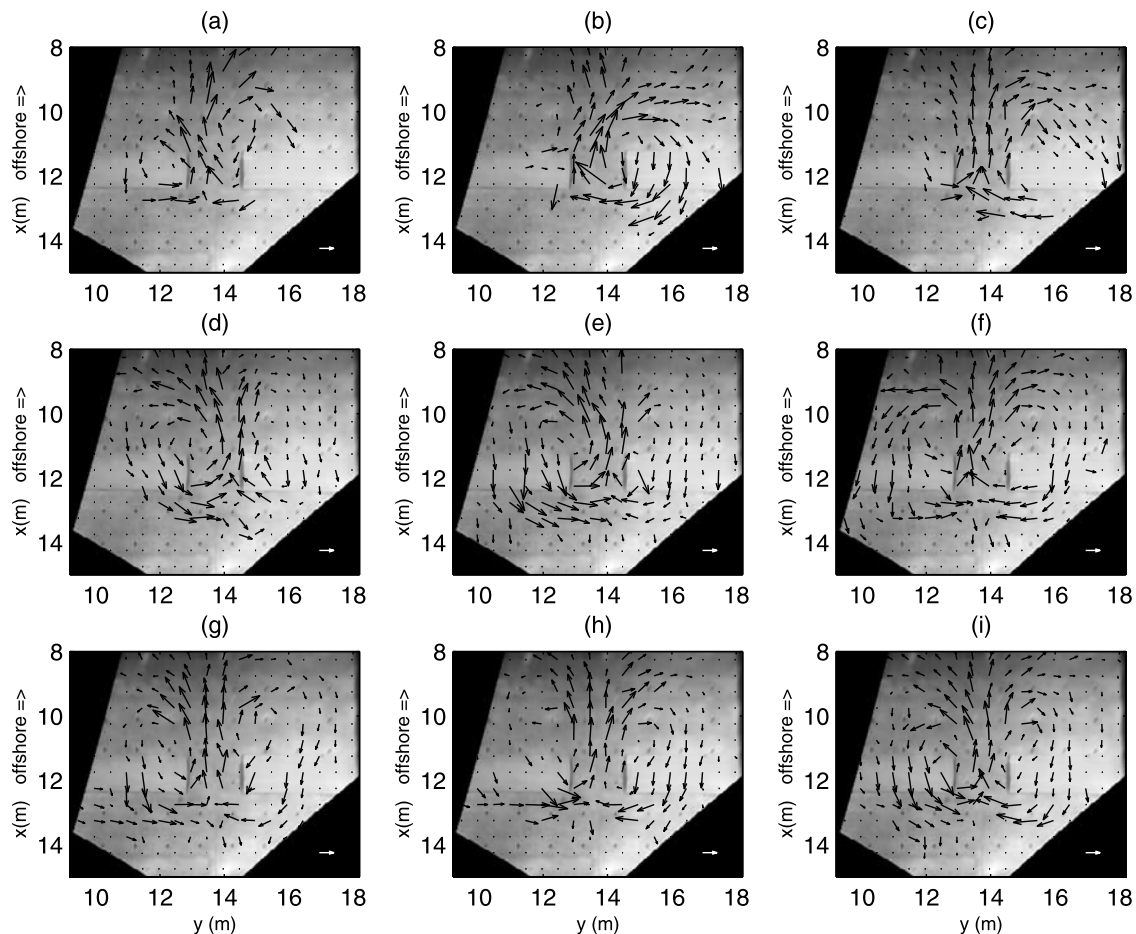


Figure 6. Two minute averages of drifter velocities over the first 18 min of test G32L1M.

1999; Yu and Slinn, 2003; Haas et al., 2003], and large, transient vortices have also been associated with field rip currents by Smith and Largier [1995].

[25] For unsteady wave tests, oscillations in current strength were visible on the wave group scale, although they are unresolvable on our figures. Often, a group of drifters was ejected offshore just before the low point of the wave group. This quick acceleration appeared to be related to both the large velocity in the rip neck at this time and the small opposing Stokes drift from the smaller waves in the group.

[26] Turbulent effects were obvious from inspection and some patterns were noticeable. The smallest eddies of $O(0.5 \text{ m})$ were most common in the unsteady tests. These are generated by some combination of differential breaking on the bar and rip channel [Peregrine, 1998, 1999] and vortex shedding on the bar corners. During tests with unsteady waves, the current velocity lagged somewhat the wave group forcing. Thus during the high point of the wave group, velocities, although accelerating strongly, could be small. This meant that differential breaking acted for longer times on a material fluid packet, producing discrete vortices instead of a sheared jet. Similar results are seen in the simplified vortex simulations of Kennedy [2003].

[27] Paths taken by drifters were dependent both on the hydrodynamics of each test and the locations where they were introduced; most drifters were introduced in the

vicinity of the rip neck and feeder currents at the rate of 6–12/min. Others were placed in other locations at more irregular intervals, mainly in areas which appeared visually to have lower drifter coverage. For the deeper water depth, drifters tended to exit the field of view to the left or to ground at the shoreline, with few traveling offshore. In contrast, for the shallower depth, many more drifters went offshore, with very few exiting to the left of the domain. These characteristics may be seen clearly in Figures 4–7.

4. Mean Properties

[28] Mean properties studied here include drifter velocity, drifter vorticity, continuity, and circulation. As noted previously, drifter velocities are not the same as would be measured by a fixed current meter but, if Eulerian velocities and Lagrangian drift do not vary strongly with depth, are a leading order approximation for the mass transport velocity used in hydrodynamic theories.

[29] We also note again the very long period oscillations found in some tests. Because of this, we could not capture a large number of periods, and mean values observed will be affected. This primarily applies to tests with deeper water over the bar and at locations offshore of the rip channel. For velocity oscillations with form $u' = A \cos(\sigma t + \epsilon)$ and a record length T , the ensemble-averaged RMS error in mean velocity caused by a finite record length will be

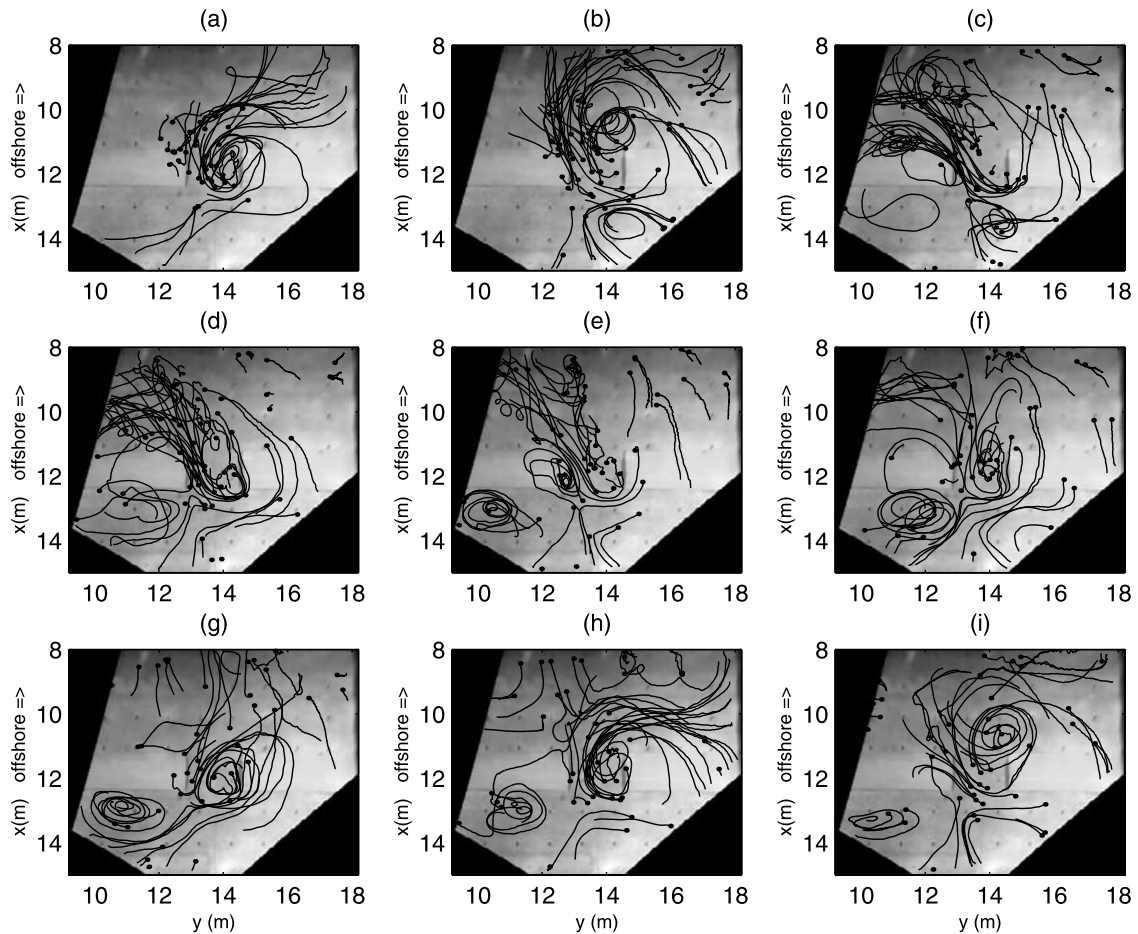


Figure 7. Two minute drifter tracks over the first 18 min of test SH267M. Dots indicate track beginnings either at start of each 2 min period or when drifter was introduced.

$\langle \delta u \rangle = A\sqrt{1 - \cos \sigma T} / \sigma T$. For the worst case scenario here, with an oscillation period of 25 min and a record length of 18 min, the RMS error in computed mean velocity will be around 0.23 of the amplitude of the oscillation. For shorter oscillation periods, error decreases quickly. If oscillations are very long, errors are not negligible, but neither do they seriously imperil the computation of mean velocities.

4.1. Continuity

[30] Taking the time average of the mass conservation equation

$$\frac{\partial \eta}{\partial t} + \nabla \cdot [(h + \eta)\mathbf{U}] = 0, \quad (3)$$

where \mathbf{U} is the mass transport velocity, gives

$$\nabla \cdot \overline{[(h + \eta)\mathbf{U}]} + \nabla \cdot \overline{[\eta'\mathbf{U}']} = 0, \quad (4)$$

where primes denote fluctuating components and overlines denote time averages. As we are unable to measure either mean or fluctuating surface elevations over the domain, we introduce some additional error by assuming that all time averages associated with surface elevations are zero and still more by approximating mass transport velocities by drifter

velocities. Rough estimates of the error introduced by approximating the mean water level by the still water level using data from *Haller et al.* [2002] and *Haas and Svendsen* [2002] gives divergence velocity errors of $O(0.025 \text{ cm/s})$, which are negligible compared with other error sources. Mean drifter velocities are computed using the approach to be described in section 4.2.

[31] Now we are able to compute the divergence of mass flux based on drifter studies for all tests. Figure 8 shows computed divergence of mass flux for test SH1L. Random errors are visible everywhere, but systematic errors are seen offshore of the rip neck. Here, divergences are strongly positive with magnitudes of several cm/s , which were by far the largest of any test. Thus more mass appears to be leaving any control volume here than enters. This is due to differences between computed mean drifter velocities and the depth-averaged mass-transport velocity (as the time average of the mass-transport flux has zero divergence by definition).

[32] An estimate of the relative errors in the mass transport flux over the entire domain may be found from the ratio of divergence velocity and drifter velocity scales: i.e., $|\nabla \cdot (h\mathbf{U}_D)|_{RMS} / |\mathbf{U}_D|_{RMS}$. Table 2 shows this quantity using as the domain all locations where both mean drifter velocities and divergences were computed. RMS divergence velocities range from 4.5–9% of RMS mean horizontal velocities

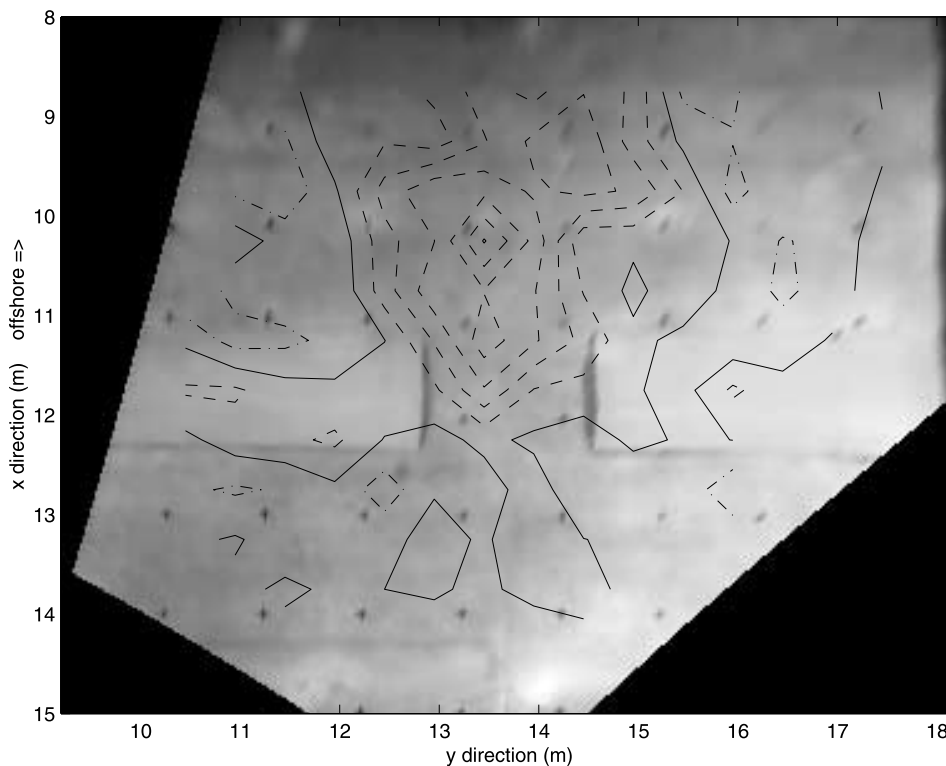


Figure 8. Divergence of mean volume flux for test SH1L. Contour interval is 0.5 cm/s. Solid line is zero; dashed line is positive divergence; dash-dotted line is negative divergence.

with tests G32H1M and SH1L showing the largest relative errors. This is an incomplete measure of accuracy, as it does not identify the sources of these errors but does show that they are on average an order of magnitude smaller than mean velocities. However, just offshore of the rip channel they may have local importance.

[33] There are several likely reasons for these nonzero divergences: wave Lagrangian drift, three-dimensional effects, nonzero correlations between fluctuating drifter concentration and velocity, and effects of finite drifter size in locations with strong flow gradients. Stokes drift can produce divergences through depth-varying and finite amplitude effects. Particularly near the rip channel, finite amplitude effects are likely significant. Depth varying currents are certain on this topography, as shown by *Haas and Svendsen* [2002], and would produce divergences resembling those observed here. Velocity-concentration effects are extremely difficult to quantify, as this is essentially a turbulent closure problem. As considerable velocity fluctuations were observed on this topography, they are likely to have some effect on divergences. Divergences due to finite drifter size are possible but are likely small.

4.2. Drifter Velocities

[34] Mean drifter velocities were obtained using a standard binning approach. In this, the rectified domain was divided into $0.5 \text{ m} \times 0.5 \text{ m}$ bins. Whenever a drifter was in one of these bins, its velocity was added to a running total for the bin. The final value for each bin was then divided by the number of observations to arrive at a mean velocity. Using observations separated by $1/3 \text{ s}$, a minimum

of 20 observations of drifter velocities in a bin were required for the mean velocity to be accepted. Results are to be presented for mean measured drifter velocities, which can differ from mean Eulerian velocities. In this section we present means for the entire test; 2 min means were given in Figures 4 and 6, which used a lower threshold of five observations.

[35] Aside from usual considerations of statistical significance from limited observations, binning approaches can have additional biases [see, e.g., *Garrafo et al.*, 2001]. If the drifter concentration per unit surface area is given by C , then the binning approach implicitly assumes

$$\overline{U'_D C'} = 0, \quad (5)$$

where primes indicate unsteady components and the overbar denotes time averaging. Thus if fluctuating drifter concentrations and velocities are related, the estimate will be biased. In these experiments, there is certainly some

Table 2. Relative Mass Flux Divergences in a Rip Current System

Test	$ \nabla \cdot (h\overline{U}_D) _{RMS}/ \overline{U}_D _{RMS}$
G32H1M	0.071
SH1M	0.053
G32L1M	0.060
SL1M	0.049
SH1L	0.089
SL133L	0.045
G64H1M	0.061
SH267M	0.055

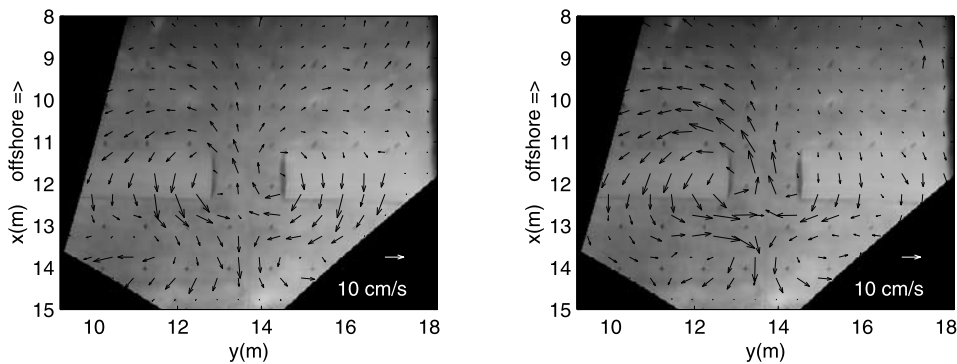


Figure 9. Mean drifter circulation for cases G32H1M and SH1M.

unknown correlation; an examination of Figure 4 shows that there are few drifters in the top right portion of each subplot except when the rip direction is to the right. As the cell-scale changes correspond to shifts in velocity (e.g., Figure 5), a bias in mean velocities seems likely, although quantifying this bias seems difficult in the general case.

[36] Figures 9–12 show mean drifter velocities for all tests. They show broad similarities: feeder currents, strong offshore velocities around the rip channel, recirculation cells to the left and right of the rip channel facing offshore, and additional circulation cells behind the bar. However, details differ considerably. In several of the tests, rip currents as they head offshore are seen to be noticeably asymmetric. These appear to be water level dependent; rips tending to the left going offshore appear only for a depth over the bar of 4.73 cm, while the one strong right case appears for the lower water level. Although some part of these asymmetries may be attributable to a finite sample length, a left asymmetry for tests similar to SH1M has been noted previously by *Haller et al.* [2002] and *Haas et al.* [2003]. *Haas et al.* found that for this topography, the basin varied in depth by around 1 cm in the longshore. Differential breaking caused by this depth variation was hypothesized to be the source of the bias, as would be predicted by theory [e.g., *Peregrine*, 1998, 1999]. However, the huge rightward asymmetry found here in test SL133L appears opposite to this trend, and its cause has remained elusive. (Further unpublished tests by K. A. Haas and A. B. Kennedy (unpublished report, 2002) confirm this bias to be both real and persistent.) Occasional gaps in coverage or strange velocity fields

further offshore, found in several tests, are functions of the finite numbers of drifters and test lengths.

[37] Velocity comparisons here show results arising from these differences. Figure 13 shows cross-shore velocities along the centerline of the rip channel. All tests show shoreward currents onshore of the bar and offshore currents in deeper water, as were seen in Figures 9–12. The locations of peak offshore-directed drifter velocities span a range from $9.75 \text{ m} < x < 12.25 \text{ m}$, with stronger rips tending to have their peak velocities further offshore from the bar crest. Water level effects are readily apparent when comparing deeper water tests [SH1M, G32H1M, G64H1M] to low water tests [G32L1M, SL1M]. All of these have similar wave heights and identical periods, but low water cases have much stronger currents. The low water test SL133L, with a slightly larger wave height and different period, has the strongest velocities of all tests. These stronger velocities for lower water levels over the bar are in agreement with *Brander and Short* [2001], *Haller et al.* [2002], and others.

[38] Wave height effects may be observed by comparing tests SH1M and SH1L, which shows a strong increase in rip strength with increasing wave height, as expected. An increase in rip current strength with wave height has also been observed by *Brander and Short* [2001], *Haller et al.* [2002], *Yu and Slinn* [2003], and others.

[39] Wave group effects may be estimated by comparing test SH1M with G32H1M and G64H1M and test SL1M to G32L1M. For all direct comparisons, drifter velocities from steady cases appear somewhat stronger than for unsteady cases, but the effect is much less than results from changing

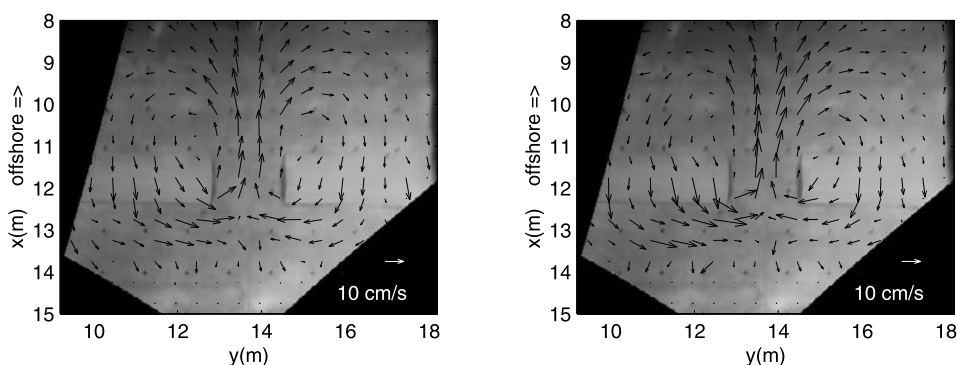


Figure 10. Mean drifter circulation for cases G32L1M and SL1M.

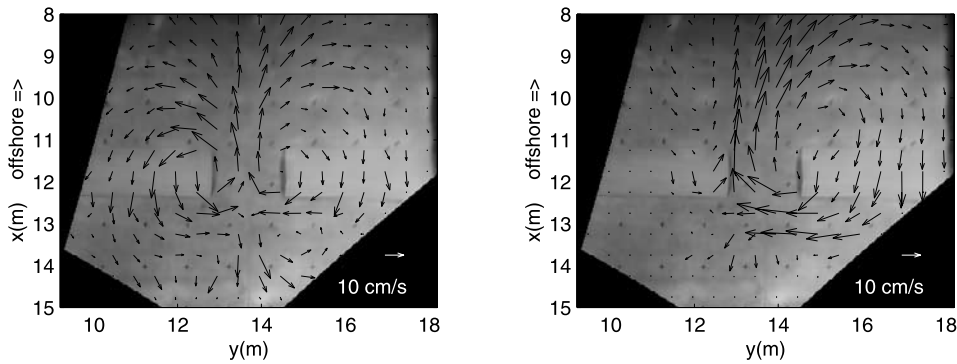


Figure 11. Mean drifter circulation for cases SH1L and SL133L.

water levels and wave heights. It is difficult to tell exactly how much significance to give this, as correlation between unsteady Stokes drift and current velocity in the rip channel was visibly nonnegligible and had some effect on unsteady tests. Tests SH1M and SH267M, which have similar wave heights and water levels but different periods, also have a similar current profile. Thus wave periods may also be of secondary importance.

[40] Wave and Eulerian current meter measurements were also taken but were never simultaneous with drifter tests, as fixed measurement equipment would interfere with the drifters. Drifter velocities may be compared with ADV measurements in the rip channel to get an estimate of other processes affecting the drifters. As currents in the rip neck are expected to be more or less depth-uniform [Haas and Svendsen, 2000], we may estimate the Lagrangian Stokes drift on the drifters using equation (1). Comparing drifter velocities here with ADV measurements is a near-worst case scenario, as waves in the rip channel were often very large and occasionally broke near the ADVs. Visually, the influence of the waves was obvious, and drifters that approached the rip neck from feeder channels would slow down considerably, sometimes stopping altogether. In unsteady tests, waves could often make it offshore only during the lower portion of the wave group. If the drifter made it offshore of around $x = 11$ m, it would accelerate strongly, as waves here were considerably smaller.

[41] Stokes drift was estimated by decomposing ADV data into wave and current components using low-pass and high-pass filters. The magnitude and phase of the cross-

shore orbital velocities, combined with the instantaneous current magnitude, could then be found at any time to give a time series of wave height, direction, and wave number. Because of wave blocking considerations, a maximum current strength of 35 cm/s was imposed, and physical limitations and occasional velocity spikes dictated a cutoff maximum wave height of 10 cm. These limitations were invoked very infrequently and are believed to have a negligible influence on computed mean Stokes drift. Waves were also assumed to travel only in the positive x -direction as longshore orbital velocities showed considerable noise.

[42] Lagrangian drift evaluated at the still water level could then be estimated at any time using a small-amplitude relation

$$U_{SL} = \frac{ga^2k \coth(2kh)}{C} \quad (6)$$

in the direction of the wave, where a is the wave amplitude and C is the phase speed [e.g., Dean and Dalrymple, 1984]. The mean of the computed surface drift time series was then subtracted from the drifter mean velocity. This small-amplitude relation will show some error as waves become large but may be acceptable as a first approximation. This is essentially a conversion from the surface Lagrangian velocity (which is the leading-order approximation to the mass transport velocity) to Eulerian velocity, which is measured by current meters.

[43] Figure 14 and Table 3 show mean drifter velocities from a bin centered in the middle of the rip channel at

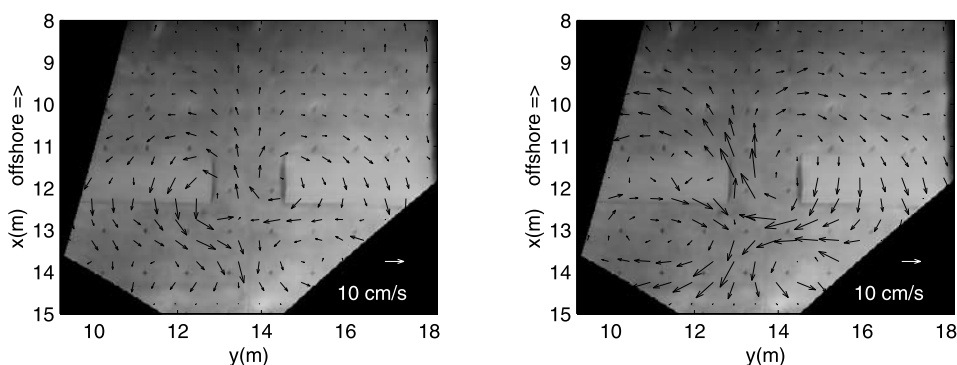


Figure 12. Mean drifter circulation for cases G64H1M and SH267M.

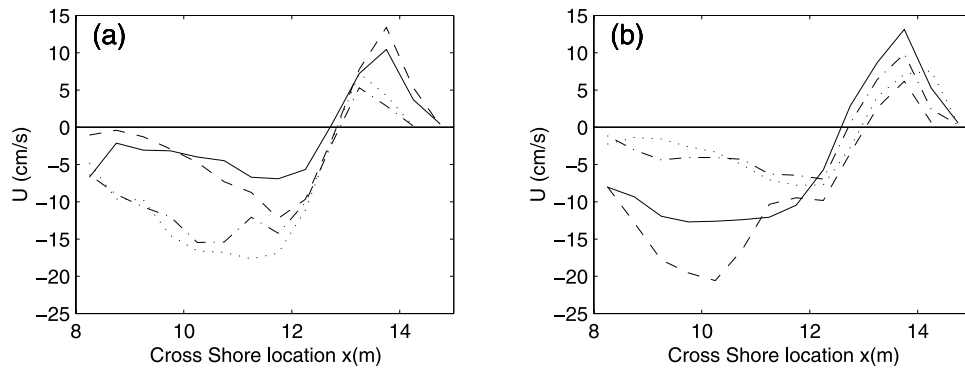


Figure 13. Centerline cross shore mean velocities for (a) Tests (solid line) G32H1M; (dashed line) SH1M; (dash-dotted line) G32L1M; (dotted line) SL1M. (b) Tests (solid line) SH1L; (dashed line) SL133L; (dash-dotted line) G64H1M; (dotted line) SH267M.

$x = 11.8$ m around the three ADVs, with a longshore width of 50 cm, and cross-shore width of 10 cm. Differences between measured drifter and current meter mean cross-shore velocities are obvious and substantial and arise from the surface Lagrangian wave drift. Mean longshore velocities are much more comparable, as wave drift is much smaller in this direction. Cross-shore drifter velocities show much better agreement with Eulerian ADV measurements after subtracting computed Stokes drift. The RMS difference between Lagrangian and Eulerian measurements then decreases from 6.8 cm/s to 3.3 cm/s, and the systematic bias seems to have disappeared. Longshore velocities were not modified for Stokes drift and have a RMS difference of 1.8 cm/s, with no obvious systematic bias. These show that for large waves (near bar, rip channel, and shoreline), Lagrangian wave drift must be taken into account if accurate comparisons are to be made between drifters and other types of measurements. However, this is just where small-amplitude approximations to Stokes drift may show considerable error. Still, as shown in Figure 14, they may provide an adequate approximation. Offshore of the bar, Stokes drift will be much smaller and may be negligible in some cases.

4.3. Circulation

[44] There has never been a consensus on how to quantify simply the driving forces behind rip currents. There

is agreement that the overall offshore mass transport in the rip must be balanced by the overall onshore mass transport over a bar or shoal, but this is simply a kinematic expression of mass conservation, not a dynamic forcing argument.

[45] By assuming that the total onshore mass transport per unit bar length was equal to the depth-integrated Stokes drift plus breaking-induced roller transport, several authors [Aagaard *et al.*, 1997; Brander and Short, 2001] have used the kinematic expression of mass conservation to estimate total offshore mass transport in a field rip current. Although reasonable agreement was found at the location considered, this argument (which we will call the “mass transport hypothesis”) has considerable theoretical difficulties.

[46] This may be illustrated by a simple thought experiment; imagine a rip channel system where the longshore length of the bar goes to infinity when compared with the width of the rip channel. The mass transport hypothesis would suggest that the rip channel velocity will also go to infinity, but this will not happen. Instead, as the bar length increases, an increasing proportion of the computed mass transport returns over the bar as undertow, and the flow through the rip channel remains approximately constant. This has been demonstrated by Svendsen *et al.* [2000], who found that the total volume flux through a rip channel does not depend on the length of the bar, a finding which contradicts the mass transport hypothesis.

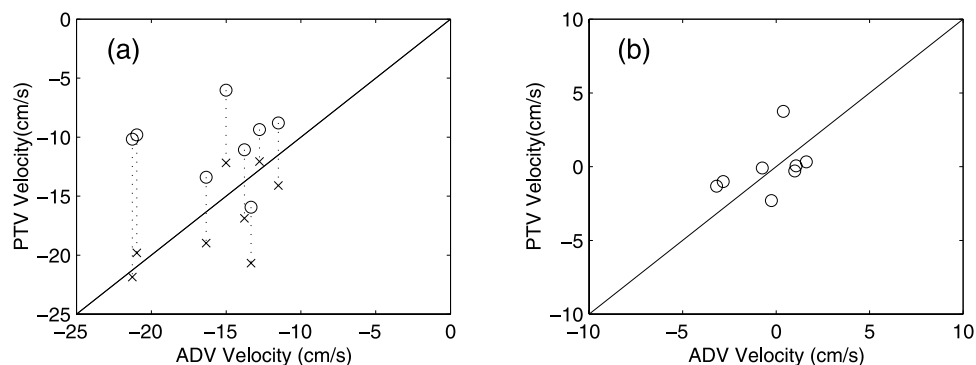


Figure 14. Mean velocities in rectangle extending 5 cm in all directions past locations of three ADVs. (a) Cross-shore velocity; (b) longshore velocity. Circles indicate no correction for Stokes drift; crosses indicate corrected for Stokes drift.

Table 3. Measured Drifter and Current Meter Mean Velocities and Computed Mean Stokes Drift in the Rip Channel

Test	Cross-Shore Velocities, cm/s			Longshore Velocities, cm/s	
	Current Meter	Stokes Drift	Drifter	Current Meter	Drifter
G32H1M	-15.0	6.2	-6.0	-3.2	-1.3
SH1M	-16.3	5.6	-13.4	-2.8	-1.0
G32L1M	-13.3	4.7	-15.9	3.9	3.7
SL1M	-13.8	5.8	-11.1	1.1	0.1
SH1L	-21.0	10.0	-9.8	1.0	-0.3
SL133L	-21.3	11.7	-10.2	-0.3	-2.3
G64H1M	-11.5	5.3	-8.8	1.6	0.3
SH267M	-12.8	2.7	-9.4	-0.7	-0.1

[47] For specific geometries, scaling relationships such as representative wave heights to representative water depths can give good correlations between measured waves and currents [Haller *et al.*, 2002; Drønen *et al.*, 2002]. These can demonstrate phenomena such as increasing rip current strength with increasing wave height and decreasing water depth and are quite useful in establishing general modes of rip current behavior. Their major drawback is that correlations are derived for a particular geometry and are relatively difficult to extend to other situations.

[48] The question of rip forcing is then often taken to be the result of wave-induced radiation stresses which force water levels and currents [Haas *et al.*, 2003; Yu and Slinn, 2003]. Here, the system looks like

$$\frac{\partial \mathbf{U}}{\partial t} + \mathbf{U} \cdot \nabla \mathbf{U} + g \nabla \eta + \frac{1}{h + \eta} \nabla \cdot \mathbf{S} + \mathbf{MIX} + \mathbf{BF} = \mathbf{0}, \quad (7)$$

where $\mathbf{U} \equiv \overline{\mathbf{M}/(h + \eta)}$ is the depth-averaged mass transport velocity which by definition includes both Eulerian and Lagrangian components, \mathbf{M} is the total depth-integrated volumetric transport, \mathbf{S} is the 2-D radiation stress tensor, η is the wave-averaged free surface elevation, and \mathbf{MIX} and \mathbf{BF} are schematics for various momentum mixing terms and bottom friction, respectively. (Note again that in shallow water for depth-uniform flow and with the small-amplitude approximation to Stokes drift, the mass-transport velocity is equal to the drifter velocity for nonbreaking waves. Hence measured drifter velocities would seem to be a good first approximation to the mass-transport velocities.)

[49] Using formulations like this, rip current forcing can then be shown to result from lateral variations in height along wave crests arising from wave breaking [Bowen, 1969]. This is theoretically sound and forms the basis for most modern computational techniques, but simple predictive estimates of forcing are difficult, as details of wave breaking and other transformations are required over an area encompassing the bar and rip channel.

[50] An alternate point of view is given by Peregrine [1998, 1999], who suggested that direct rotational forcing might be a better way of examining vortical flows (like rip currents) in the nearshore. Circulation in shallow water flows, defined as $\Gamma \equiv \oint \mathbf{U} \cdot d\mathbf{l}$, is conserved along any material circuit (neglecting bottom friction) in the absence of wave breaking. For breaking waves, circulation can only be generated when the strength of breaking varies along a wave crest. This applies directly to rip currents, where wave breaking on the bar is strong but may be zero in the rip channel. Most importantly, if there is no breaking in the rip

channel, the instantaneous rate of change of circulation over any closed circuit through the bar and rip channel depends only on the instantaneous rate of bore dissipation on the bar. Put more simply, circulation forcing depends only on how waves break on the bar, not on bar length or rip channel width.

[51] This lack of dependence on the details makes it easier to formulate simple dynamical estimates of rip current circulation forcing. Additionally, this approach eliminates the complicating factor of water level gradients. Following directly from Kelvin's circulation theorem, conservative forces such as the gradient of surface elevations cannot force circulation around a closed material curve, even though water level gradients may have local importance in momentum balances and will act to conserve existing circulation. Instead, circulation here is forced directly by lateral variations in breaking intensity.

[52] Peregrine's [1998, 1999] results are for bore theory, where breaking locations and integrals of evolution in space can be difficult to estimate. To circumvent this, Brocchini *et al.* [2004] considered generation of circulation using phase-averaged arguments and simple breaking models. For waves obeying the simple phase-averaged energy equation

$$\frac{\partial E}{\partial t} + \nabla \cdot (E \mathbf{C}_g) = -DhC_g \quad (8)$$

(where E is the kinematic wave energy density (energy density divided by fluid density), C_g is the group velocity, h is the water depth, and D is related to wave energy dissipation), the rate of change of circulation over a closed material circuit is

$$\frac{D\Gamma}{Dt} = \oint n \mathbf{D} \cdot d\mathbf{l}, \quad (9)$$

where $\Gamma \equiv \oint \mathbf{U} \cdot d\mathbf{l}$ is the circulation, $n \equiv C_g/C$ and $\mathbf{D} = D(\cos\theta, \sin\theta)$.

[53] For shore-normal waves breaking on a wide bar but not in a rip channel, the rate of change of circulation was estimated as

$$\frac{D\Gamma}{Dt} = \frac{5g\gamma^2}{16} (h_B - h_c) + \frac{gh_c}{8} (\gamma^2 - \beta^2), \quad (10)$$

where h_B and h_c are the depths of breaking and the depth over the bar, respectively, the breaking wave height on the bar slope is $H_B = \gamma h_B$, and the wave height at the shoreward end of the bar crest is $H_c = \beta h_c$. Here, we use $\gamma = 0.78$ and

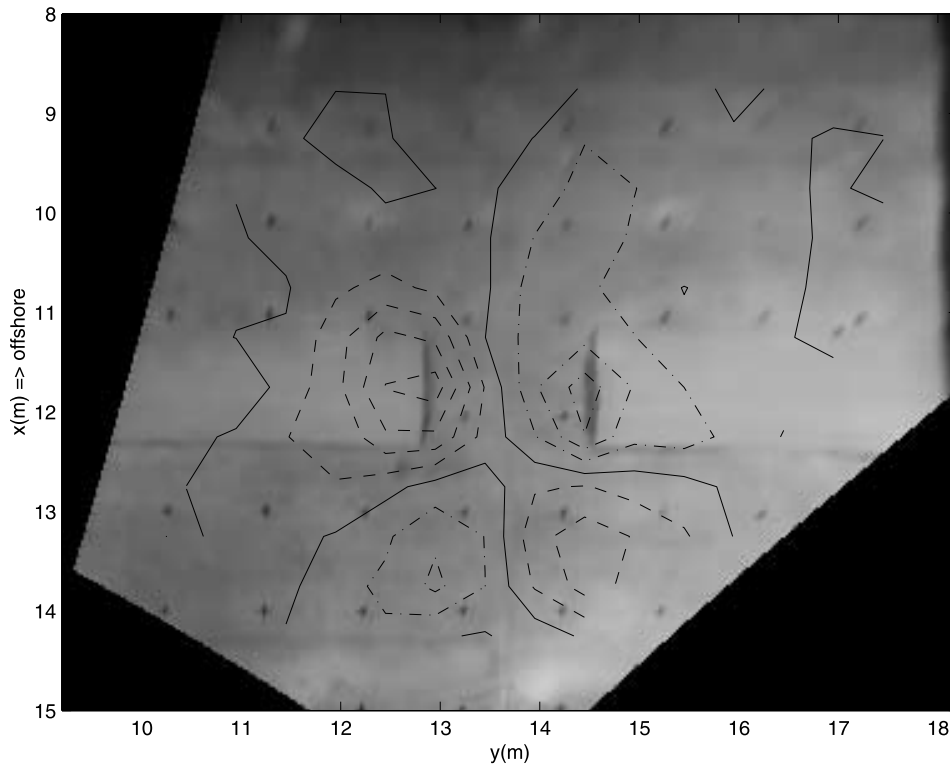


Figure 15. Mean drifter vorticity for case SH1L. Contours are spaced every 0.1 rad/s. Four distinct circulation cell quadrants are visible.

$\beta = 0.45$ for all cases. The breaking depth for shore-normal waves may then be estimated as [e.g., *Dean and Dalrymple, 1984*]

$$h_B = (H_0^2 C_{g0})^{2/5} \gamma^{-4/5} g^{-1/5}. \quad (11)$$

Comparisons of this and other estimates with directly measured rates of circulation change at startup showed good agreement, although considerable scatter was apparent (A. B. Kennedy et al., Topographically controlled, breaking wave-induced macrovorticities, part 2, Rip current topographies, submitted to *Journal of Fluid Mechanics*, 2004). This generation of circulation estimate was also used in a simplified model of a rip current neck [*Kennedy, 2003*] and showed good predictive ability.

[54] For stochastically steady-state conditions, the mean rate of change of circulation around any material curve must be zero but the mean circulation will have some finite value. Thus the dissipation of circulation by bottom friction (the only other nonconservative process for depth-uniform flow around a material curve) is equal to the generation of circulation according to equation (10). Here, we estimate the mean drifter circulation around a circulation cell and compare it with the computed generation of circulation. There are several difficulties. First, as there is a limited field of view, all estimates of drifter circulation will be low, particularly for stronger rips, which extend further offshore. Second, the curve should follow a moving material surface, but we must approximate this using a fixed dividing streamline. Use of a fixed curve introduces error when there is unsteady flow and mixing occurs between the two circulation cells but it is not technically feasible to follow a material surface.

[55] Dividing streamlines may be obtained by an examination of mean drifter vorticity, computed as $\omega = \partial V/\partial x - \partial U/\partial y$. Figure 15 shows computed drifter vorticity for test SH1L, which is typical in pattern, and shows processes clearly. Four quadrants of circulation may be seen, with two dividing streamlines. From the middle of the trough to the offshore extent of the boundary, symmetric positive and negative circulation cells may be seen with a dividing streamline near the center of the rip channel. Closer to the shoreline, two more symmetric cells are seen. In all tests, the strongest vorticity was near the bar-rip channel boundary, as expected.

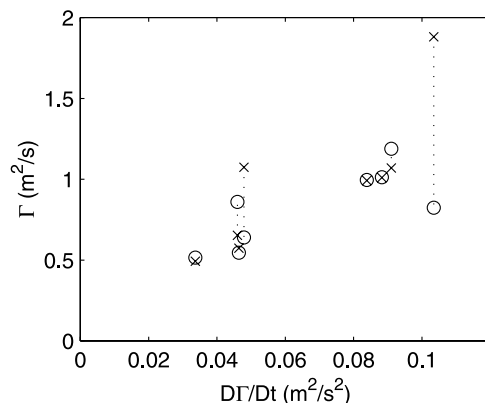


Figure 16. Dimensional production of circulation compared to measured circulation about mean circulation cells. Crosses indicate negative circulation cell; circles indicate positive circulation.

Table 4. Computed Generation and Dissipation Scales Using Bottom Friction $c_f = 0.039$

Test	$D\Gamma/Dt \text{ m}^2/\text{s}^2$	$\Gamma, \text{m}^2/\text{s}$		Dissipation of $\Gamma, \text{m}^2/\text{s}^2$	
		Positive	Negative	Positive	Negative
G32H1M	0.046	0.55	0.57	0.026	0.031
SH1M	0.046	0.86	0.65	0.047	0.034
G32L1M	0.088	1.01	1.01	0.052	0.051
SL1M	0.091	1.19	1.07	0.096	0.079
SH1L	0.084	1.00	0.99	0.082	0.065
SL133L	0.104	0.82	1.88	0.054	0.174
G64H1M	0.034	0.51	0.49	0.029	0.023
SH267M	0.048	0.64	1.07	0.033	0.055

[56] All of these cells are generated by gradients in breaking along wave crests; strong breaking on the bar and weak or no breaking in the channel generates the deeper cells, while strong breaking shoreward of the rip channel and weak shore breaks between the bars and shoreline generate the shallower cells. For tests where the mean rip direction is asymmetric, four-quadrant circulation is still visible but the dividing streamline is also biased left or right.

[57] By following these dividing streamlines (with some allowance for irregularities), circulation was computed in the offshore cells by interpolating mean velocities and integrating along a polygon approximating the dividing streamline. Figure 16 and Table 4 give computed circulation forcing against measured circulation for all cases where a reasonable estimate could be made. These are given dimensionally, as generation and dissipation scalings differ and the proper choice is unclear.

[58] Several observations are immediate. First, for most tests, positive (counterclockwise) and negative (clockwise) circulation cells have very similar strengths, even when the rip shows a significant bias. This was expected from equation (10), but confirmation is welcome. A notable exception is case SL133L. Here, because of spotty coverage on the left side of the domain, a poor estimate was made for the positive circulation cell. Case SH267M, a case with a strong asymmetry in mean drifter velocities, also shows differences in positive and negative circulation cells.

[59] The second point of interest is that steady circulation increases strongly with computed forcing, although scatter is apparent. This increase in circulation can come from two possible sources: velocities may increase with increasing forcing and the circulation cell may extend further offshore. Examination of Figures 9–12 shows that rip currents with large velocities also tend to travel further offshore, which is not intuitively surprising.

[60] As these results include both steady and unsteady waves, two water levels, three wave periods, and many wave heights, the strong relationship between predicted forcing and measured mean circulation is highly encouraging. The form of this relationship will depend on bottom friction, the relationship of circulation cell area to forcing, and other factors which are not well understood. However, the existence of a relationship between forcing and mean circulation appears strong. For the simpler case of velocities in the rip neck, Kennedy [2003] showed that generation of circulation arguments could provide direct quantitative predictions of several steady and unsteady properties, but the case of total rip current circulation considered here is considerably more complex.

[61] On the basis of the measured mean circulation and estimated generation of circulation, rip current time scales may be computed as $T_{circ} = \Gamma/(D\Gamma/Dt)$. This is an estimate of the spin-up time for the rip current to reach full circulation. It is certainly an underestimate, as mixing between positive and negative circulation cells, limited field of view, and bottom friction effects are neglected. Still, it may give a reasonable estimate of characteristic time scales of rip current circulation. Figure 17 shows this quantity, which appears to be fairly constant. It is quite small; for the physical experiments, this comes to around 15 s, possibly decreasing weakly as rip strengths increase. Even if this is an underestimate by a factor of four (which seems unlikely), this would only be around 60 s! We are not suggesting that the rip reaches steady state in this time but rather that the mean circulation in the rip current system is relatively small when compared with the rate of generation of circulation.

[62] Using Froude scaling to move up to full scale and using a length scaling factor of 36 (time scale factor of 6), this suggests that the rip current cells may respond over 360 s at maximum and 90 s at minimum. These overlap the time scales of wave groups and thus provide reasons for the overwhelming anecdotal, field, and laboratory evidence that rip currents respond strongly to unsteady wave forcing [Shepard and Inman, 1941; Sonu, 1973; Kennedy and Dalrymple, 2001].

[63] It is possible to estimate the dissipation of circulation directly from drifter measurements, as the only sink for circulation in steady, depth-uniform shallow water flows

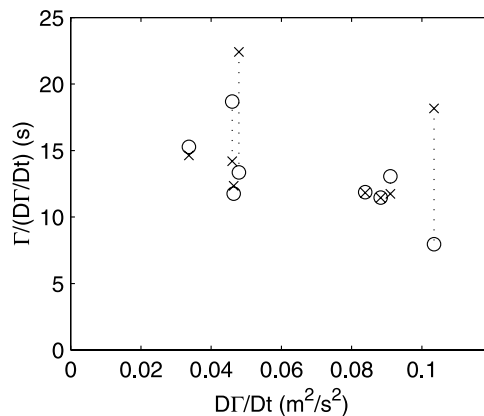


Figure 17. Time scales for generation of circulation in a rip current cell. Crosses indicate negative circulation cell; circles indicate positive circulation.

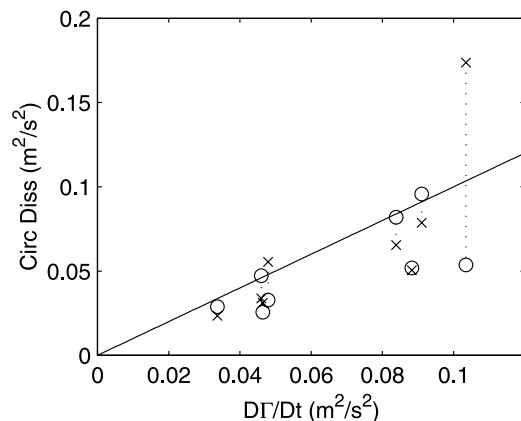


Figure 18. Dissipation of circulation from bottom friction using best fit $c_f = 0.039$. Crosses indicate negative circulation cell; circles indicate positive circulation. Line indicates perfect agreement.

comes from bottom friction. (If flow is not depth-uniform or steady, other processes such as depth-uniform and depth-varying mixing are also important, which applies in some measure offshore of the bar.)

[64] We take the mean bottom frictional force as

$$\overline{\mathbf{F}_b} = c_f \rho \overline{\mathbf{U}_B |\mathbf{U}_B|}, \quad (12)$$

where c_f is a frictional coefficient and \mathbf{U}_B is the low-pass bottom velocity. This approximation neglects the influence of wave orbital velocities, so for a given frictional coefficient, bottom stress is likely to be underestimated somewhat using this formulation. Alternatively, given an estimate of the mean stress, the frictional coefficient is likely to be overestimated. Here, we will approximate the bottom velocity by the drifter velocity which again introduces error where there is strong Stokes drift and/or depth-varying velocity.

[65] The instantaneous dissipation of circulation over a closed curve (which is equivalent to the area integral of the vorticity dissipation) due to bottom friction may then be computed as

$$\frac{D\Gamma}{Dt_{bf}} = - \oint \frac{c_f}{h} \mathbf{U}_D |\mathbf{U}_D| \cdot d\mathbf{l}. \quad (13)$$

We approximate the time-averaged dissipation of circulation by computing the time average of this quantity, but about a fixed closed curve, and using dividing streamlines to separate circulation cells. This introduces some additional error, as it is not a material surface, but is a necessary approximation.

[66] Figure 18 and Table 4 give the computed rate of circulation generation using equation (10) against the measured rate of circulation dissipation using equation (13). Using a best fit value of $c_f = 0.039$ for the frictional coefficient, good agreement is obtained for everything except test SL133L. The coefficient used appears somewhat high, although still the correct order of magnitude. Some possible reasons for this include (1) neglect of wave orbital velocities on bottom friction (makes c_f estimate higher than actual value), (2) differences between drifter velocities and bottom velocities (uncertain influence on c_f), (3) limited

field of view, but visible domain is assumed to include all dissipation (makes c_f estimate higher than actual), (4) use of a fixed curve instead of a material surface when computing time averages (makes c_f estimate higher than actual), (5) nonconstant c_f or unsuitability of equation (12) (uncertain), (6) errors in estimating generation of circulation (uncertain), and (7) depth-varying velocities (uncertain). All are likely to have some influence but are difficult to quantify. Still, we see a strong correlation between predicted generation of circulation and dissipation.

5. Conclusions

[67] Overall, the use of Lagrangian drifters in this study was successful. Drifter paths showed clearly many features of the rip current including recirculation cells, vortex generation and shedding, and low-frequency cellular-scale oscillations. Maps of mean rip current velocity showed strong qualitative and quantitative differences as wave forcing and water levels were changed. Total measured mean circulation and frictional dissipation of circulation were both found to increase strongly with computed circulation forcing, which increases with increasing wave height and decreasing crest water levels. Wave period and wave unsteadiness were found to have a secondary influence on mean circulation.

[68] For almost all tests, positive and negative circulation cells had similar strengths, even when there were strong biases in rip direction. Measured mean circulation proved to be relatively small when compared with rates of generation of circulation, confirming earlier evidence that rip currents can easily respond on the scale of wave groups.

[69] Stokes drift for large waves proved to be a significant component of drifter velocity in the vicinity of the bar and rip channel. Three-dimensional effects were also apparent as the rip traveled into deeper water but proved difficult to quantify. Finally, it appears that correlations between fluctuating drifter velocities and concentrations are nonzero and affect estimates of mean quantities.

[70] **Acknowledgments.** This work was supported by the University of Florida and by the National Oceanographic Partnership Program under grant N00014-99-1-1051. Their support is gratefully acknowledged.

References

- Aagaard, T., B. Greenwood, and J. Nielsen (1997), Mean currents and sediment transport in a rip channel, *Mar. Geol.*, *140*, 25–45.
- Bowen, A. J. (1969), Rip currents: 1. Theoretical investigations, *J. Geophys. Res.*, *74*, 5467–5478.
- Brander, R. W., and A. D. Short (2001), Flow kinematics of low energy rip current systems, *J. Coastal Res.*, *17*(2), 468–481.
- Brocchini, M., A. B. Kennedy, L. Soldini, and A. Mancinelli (2004), Topographically-controlled, breaking wave-induced macrovortices. 1: Widely separated breakwaters, *J. Fluid Mech.*, *507*, 289–307.
- Chen, Q., J. T. Kirby, R. A. Dalrymple, A. B. Kennedy, and M. C. Haller (1999), Boussinesq modeling of a rip current system, *J. Geophys. Res.*, *104*(9), 20,617–20,637.
- Dean, R. G., and R. A. Dalrymple (1984), *Water Wave Mechanics for Engineers and Scientists*, Prentice-Hall, Old Tappan, N. J.
- Drønen, N., H. Karunarathna, J. Fredsoe, B. M. Sumer, and R. Deigaard (1999), The circulation over a longshore bar with rip channels, *Proc. Coast. Sed.*, *99*, 576–587.
- Drønen, N., H. Karunarathna, J. Fredsoe, B. M. Sumer, and R. Deigaard (2002), An experimental study of rip channel flow, *Coastal Eng.*, *45*(3–4), 223–238.
- Ebersole, B. A., and R. A. Dalrymple (1980), Numerical modelling of nearshore circulation, paper presented at International Conference on Coastal Engineering, Am. Soc. of Civil Eng., Sydney.

- Garrafo, Z. D., Z. Griffa, A. J. Mariano, and E. P. Chassignet (2001), Lagrangian data in a high-resolution numerical simulation of the North Atlantic II. On the pseudo-Eulerian averaging of Lagrangian data, *J. Mar. Syst.*, *29*, 177–200.
- Haas, K. A., and I. A. Svendsen (2000), Three-dimensional modeling of a rip current system, *Res. Rept. CACR-00-06*, 250 pp., Cent. for Appl. Coastal Res., Univ. of Delaware, Newark, Del.
- Haas, K. A., and I. A. Svendsen (2002), Laboratory measurements of the vertical structure of rip currents, *J. Geophys. Res.*, *107*(C5), 3047, doi:10.1029/2001JC000911.
- Haas, K. A., I. A. Svendsen, M. C. Haller, and Q. Zhao (2003), Quasi-three-dimensional modeling of rip current systems, *J. Geophys. Res.*, *108*(C7), 3217, doi:10.1029/2002JC001355.
- Haller, M. C., and R. A. Dalrymple (2001), Rip current instabilities, *J. Fluid Mech.*, *433*, 161–192.
- Haller, M. C., R. A. Dalrymple, and I. A. Svendsen (2002), Experimental study of nearshore dynamics on a barred beach with rip channels, *J. Geophys. Res.*, *107*(C2), 3061, doi:10.1029/2001JC000955.
- Hamm, L. (1992), Directional nearshore wave propagation over a rip channel: An experiment, paper presented at International Conference on Coastal Engineering, Am. Soc. of Civil Eng., Venice.
- Holland, K. T., R. A. Holman, T. C. Lippmann, J. Stanley, and N. Plant (1997), Practical use of video imagery in nearshore oceanographic field studies, *IEEE J. Ocean. Eng.*, *22*(1), 81–92.
- Huntley, D. A., M. D. Hendry, J. Haines, and B. Greenidge (1988), Waves and rip currents on a Caribbean pocket beach, Jamaica, *J. Coastal Res.*, *4*, 69–79.
- Kennedy, A. B. (2003), A circulation description of a rip current neck, *J. Fluid Mech.*, *497*, 225–234.
- Kennedy, A. B., and R. A. Dalrymple (2001), Wave group forcing of rip currents, paper presented at Fourth International Symposium on Ocean Wave Measurement and Analysis, Am. Soc. of Civil Eng., San Francisco, Calif.
- Longuet-Higgins, M. S., and R. W. Stewart (1964), Radiation stresses in water waves: A physical discussion, with applications, *Deep Sea Res.*, *11*, 529–562.
- McKenzie, P. (1958), Rip current systems, *J. Geol.*, *66*, 103–113.
- Mei, C. C. (1983), *The Applied Dynamics of Ocean Surface Waves*, 740 pp., World Sci., River Edge, N. J.
- Noda, E. K. (1972), Wave-induced nearshore circulation, *J. Geophys. Res.*, *79*, 4097–4106.
- Peregrine, D. H. (1998), Surf zone currents, *Theor. Comp. Fluid Dyn.*, *10*, 295–309.
- Peregrine, D. H. (1999), Large-scale vorticity generation by breakers in shallow and deep water, *Eur. J. Mech. B/Fluids*, *18*, 403.
- Shepard, F. P., and D. L. Inman (1950), Nearshore circulation related to bottom topography and wave refraction, *Eos Trans. AGU*, *31*(2), 196–212.
- Shepard, F. P., K. O. Emery, and E. C. La Fond (1941), Rip currents: A process of geological importance, *Eos Trans. AGU*, *31*(4), 555–565.
- Smith, J. A., and J. L. Largier (1995), Observations of nearshore circulation: Rip currents, *J. Geophys. Res.*, *100*, 10,967–10,975.
- Sonu, C. J. (1973), Field observations on nearshore circulation and meandering currents, *J. Geophys. Res.*, *77*, 3232–3247.
- Sørensen, O. R., H. A. Schäffer, and P. A. Madsen (1998), Surf zone dynamics simulated by a Boussinesq type model, III. Wave-induced horizontal nearshore circulations, *Coastal Eng.*, *33*(2–3), 155–176.
- Svendsen, I. A., K. A. Haas, and Q. Zhao (2000), Analysis of rip current systems, paper presented at 27th International Conference on Coastal Engineering, Am. Soc. of Civil Eng., Sydney.
- Yu, J., and D. N. Slinn (2003), Effects of wave-current interaction on rip currents, *J. Geophys. Res.*, *108*(C3), 3088, doi:10.1029/2001JC001105.

A. B. Kennedy and D. Thomas, Department of Civil and Coastal Engineering, University of Florida, 313 Yon Hall, Gainesville, FL 32611-6590, USA. (kennedy@coastal.ufl.edu)